

Bootstrapping Reinforcement Learning with Imitation for Vision-Based Agile Flight

Jiaxu Xing, Angel Romero, Leonard Bauersfeld and Davide Scaramuzza
Robotics and Perception Group, University of Zurich, Switzerland

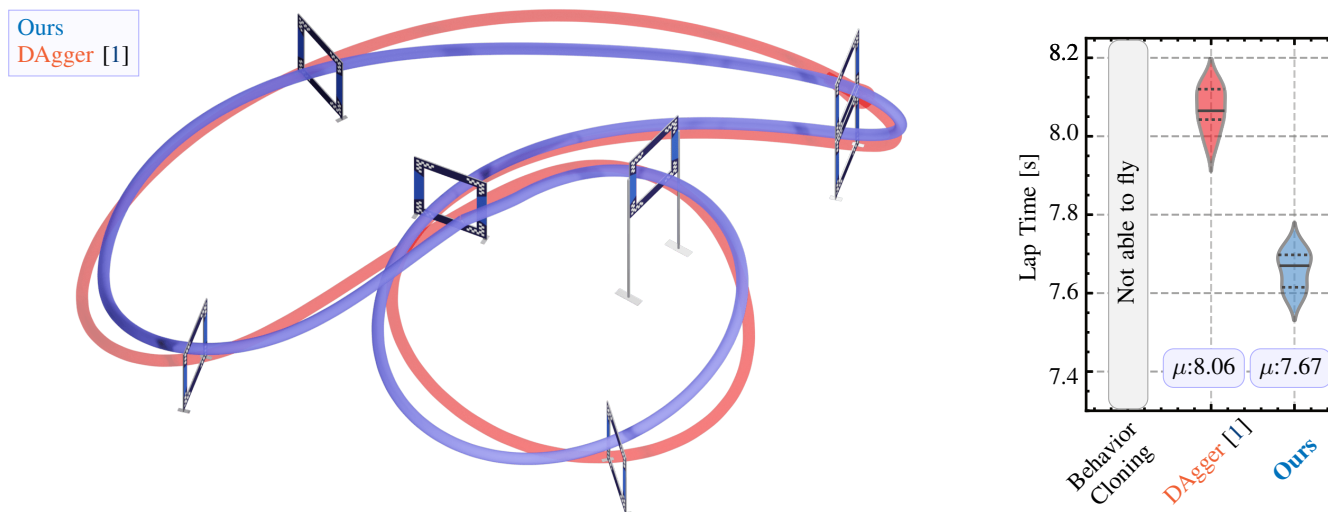


Fig. 1: *Left*: Trajectory visualization of the Imitation Learning (IL) (red) and our Reinforcement Learning (RL) fine-tuned (blue) vision-based policies from real-world, drone-racing experiments. Both policies utilize only visual observations as network inputs and can complete the race track. Trained with the same amount of data, our RL fine-tuned policy demonstrates the ability to execute tighter trajectories and fly faster. *Right*: Our policy consistently demonstrates faster flight in real-world scenarios over 10 consecutive laps, with a lap-time advantage of approximately 0.4 seconds over imitation learning alone. This margin can prove decisive in drone-racing championships where a tenth of a second can make the difference.

Abstract—We combine the effectiveness of Reinforcement Learning (RL) and the efficiency of Imitation Learning (IL) in the context of vision-based, autonomous drone racing. We focus on directly processing visual input without explicit state estimation. While RL offers a general framework for learning complex controllers through trial and error, it faces challenges regarding sample efficiency and computational demands due to the high dimensionality of visual inputs. Conversely, IL demonstrates efficiency in learning from visual demonstrations but is limited by the quality of those demonstrations and faces issues like covariate shift. To overcome these limitations, we propose a novel training framework combining RL and IL’s advantages. Our framework involves three stages: initial training of a teacher policy using privileged state information, distilling this policy into a student policy using IL, and performance-constrained adaptive RL fine-tuning. Our experiments in both simulated and real-world environments demonstrate that our approach achieves superior performance and robustness than IL or RL alone in navigating a quadrotor through a racing course using only visual information without explicit state estimation.

I. INTRODUCTION

Visuomotor policy learning enables robots to perform complex tasks by directly mapping visual information into action. This technique has been successfully demonstrated in various robotic systems to learn intricate behaviors such as visual navigation [2, 3], dexterous manipulation [4, 5], and agile

maneuvers [6, 7, 8]. The ability to learn directly from visual data allows machines to interpret visual stimuli and translate them directly into corresponding motor actions, akin to the human skill of hand-eye coordination. However, learning from only visual inputs presents an entire set of unique challenges. The intrinsic high dimensionality of visual input makes the policy exploration and learning process much less efficient compared to state-based policies with low-dimensional input. In the realm of agile quadrotor flight, these challenges are more accentuated due to its agility, inherent instability, and especially its low-level command modality: collective thrust and body rates, which require tight high-frequency closed-loop control. Previous approaches [8, 2] demonstrated success flying a quadrotor at high speeds using vision, but in all cases, the visual information was paired with high-rate proprioceptive information from an IMU for explicit state estimation. The ability of an autonomous drone to fly only from visual input without explicit state estimation and without access to IMU remains unattained.

A task that perfectly matches this set of skills is first-person-view (FPV) drone racing. When flying an FPV drone, human pilots can fly at the limits of handling while only receiving visual information at 60 Hz through a monocular camera mounted onboard the drone. In this paper, we tackle

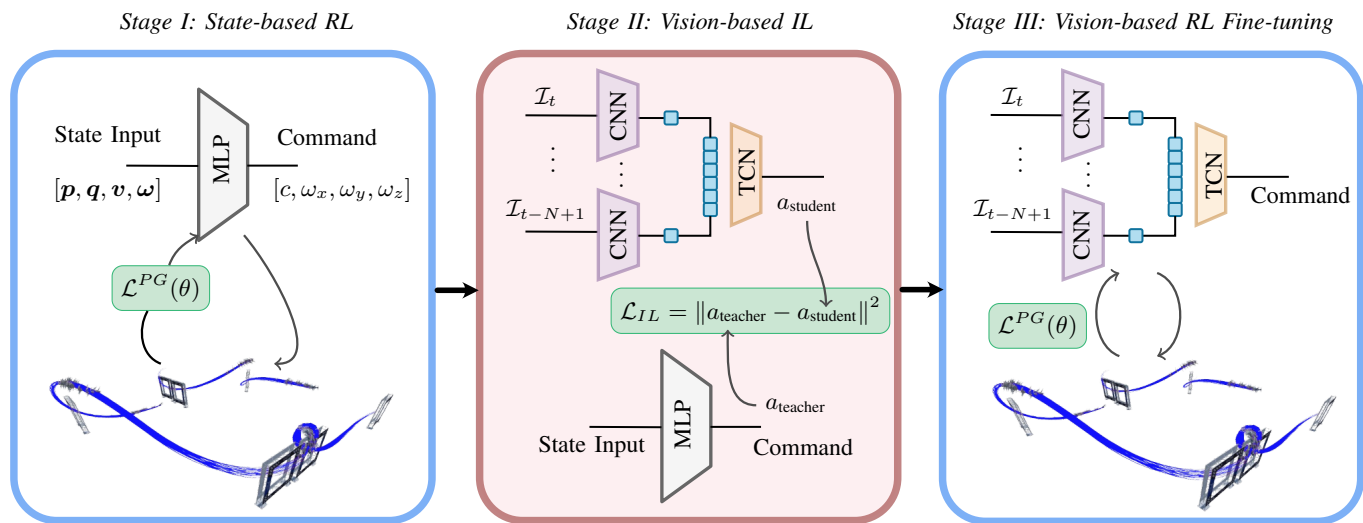


Fig. 2: Overview of our approach. We demonstrate visuomotor policy learning in three different stages. In stage I, we train a state-based teacher policy using RL. Then in stage II we used the teacher policy and perceptual inputs to perform an imitation learning. In stage III, we bootstrap the actor using the student policy from stage II and fine-tune the policy through vision-based RL.

the problem of autonomous quadrotor racing directly and only from visual input without using state estimation and IMU.

There have been primarily two approaches to this problem: Reinforcement learning (RL) and imitation learning (IL). RL is gaining traction as a general framework for designing complex controllers that are difficult to handcraft using classical methods [9, 7]. RL acquires knowledge through millions of trial-and-error interactions with a simulated environment. However, RL architectures often need to gather a large volume of data samples to effectively learn, which can be computationally expensive to generate. For this reason, the sample efficiency of RL algorithms becomes one of the most sought-after metrics. For vision-based policy learning, sample efficiency is particularly important, as (i) the dimensionality of visual observations is greatly increased, making exploration more challenging, and (ii) image rendering during interactions will significantly raise computational costs. Therefore, the task of exploring and learning *efficiently* in vision-based RL from scratch becomes crucial.

Conversely, IL has been successfully demonstrated on different mobile platforms to perform end-to-end vision-based learning [8, 2, 10, 11]. IL attempts to synthesize policies from visual demonstrations using either expert demonstrations or a privileged policy in a supervised fashion. The optimization objective is to clone an expert rather than to interact with the environment and collect rewards in RL. Due to this simplification, IL typically requires fewer samples and, consequently, has been validated for real-world robot learning problems [2, 8, 11, 10]. However, IL encounters several challenges. Among these, a significant issue is the phenomenon of *covariate shift*. This term refers to the discrepancy that arises when the data used to train a model (in this case, the demonstrations for IL) differ from the data encountered in real-world scenarios. This mismatch can lead to degraded

performance as the learned policy might not generalize well to new, unseen situations. Furthermore, another limitation of IL is that the effectiveness of the learned policy is inherently bounded by the quality of the expert policy or demonstrations. In other words, the policy derived from IL cannot outperform the demonstrations it was trained on.

In this paper, we explore the unique challenges of controlling agile quadrotors using only visual information (either from raw image pixels or image abstractions such as corner coordinates) in the context of drone racing. Drone racing pilots must navigate a quadrotor through a predefined sequence of gates as fast as possible using only onboard camera information. We chose this task because it represents the complexities of navigating quickly in complex, known environments. The large observation space, driven by rapidly changing visual data, and the need for real-time response make the drone-racing task an ideal benchmark for visuomotor policies, especially when directly controlling low-level commands such as collective thrust and body rates.

Previous work on drone racing demonstrated their superior performance of RL for state-based policy learning [7, 9] and the efficiency of IL for vision-based policy learning [12]. In this work, we showcase the effectiveness of combining the advantages of vision-based RL and IL for agile quadrotor flight to achieve more robustness and performance.

Contributions

By leveraging the complementary advantages of IL and RL, we demonstrate that the resulting policy can navigate through a sequence of gates using solely visual information *without explicit state estimation*. Our proposed training framework consists of three stages. In the initial stage, we train a teacher policy utilizing privileged state information. During the second stage, we use IL to distill the teacher policy into

a student policy. The student policy does not have access to privileged information but rather to a restricted observation space like raw image pixels or image abstractions such as gate-corner coordinates. Lastly, we employ a performance-constrained adaptive RL fine-tuning. During this stage, we first train the critic network and freeze the actor so that the critic is properly initialized. Then, we adapt the policy update step for both the critic and the actor based on the collected rewards and continue RL training until the policy performance converges. Through experiments conducted in both simulation and real-world environments, we illustrate that our approach generates policies that outperform those exclusively trained through either IL or RL when learning directly from visual input.

II. RELATED WORK

A. Vision-Based Robot Learning

Deep visuomotor policies directly map actions from visual inputs, such as RGB images [5] or depth images [2, 13]. In contrast to conventional methods, end-to-end approaches often operate without the need of environmental perception [14, 15], precise state estimation [16, 17], or motion planning [16, 17, 18]. Exploring the pixel space for mobile robots is extremely data-intensive, often requiring millions of samples. This makes sample-efficiency a critical factor in vision-based learning, where rendering time often constitutes a major bottleneck in the entire framework. Existing works have demonstrated end-to-end vision-based policies primarily through both RL and IL.

In RL, the optimization objective is based on the task configuration through rewards design, and the policy is updated through interactions with simulated environments [19]. The policy encounters both positive and negative samples during these interactions, making it more robust and generalizable to the given task setting.

In contrast, in most IL approaches, the optimization objective is the difference between the learned policy and the expert demonstrations [1, 20]. Despite having a task-centric objective, vision-based RL has predominantly found application in simulations, such as static manipulation tasks [21, 22], or video games [23], due to its sample complexity. Therefore, effective approaches for vision-based RL in mobile robots are still actively being explored.

On the other hand, due to its sample efficiency, IL has been demonstrated in end-to-end learning on many mobile platforms [8, 2, 6, 10, 11]. The simplification of learning the task solely from expert demonstrations dramatically reduces the required samples for effective training. However, IL often results in a limited understanding of the task. Due to the supervised fashion of policy training, the performance of IL policies is always capped by the teacher policies and cannot be further optimized [20].

B. RL Finetuning from Expert Demonstrations

For various robot learning applications, prior research poses the following question: How can expert demonstrations be

effectively leveraged to achieve high-performance policies? The current research in this domain can be broadly categorized into two main approaches: 1) RL with behavior cloning initialization and 2) replay expert samples during RL from scratch.

1) *Behavior Cloning (BC) initialized RL*: The core idea originates from [24], where the authors leverage expert demonstrations to train a BC policy in a supervised fashion. Subsequently, the policy undergoes a fine-tuning stage through RL. Using BC initialization, the exploration in RL states has a strong prior and the sample efficiency is largely increased. In the robot learning domain, this similar principle has been demonstrated in various works, such as car pole balancing [24], video games [25], dexterous manipulation [26], object goal navigation [27].

2) *Sample Previous Demonstration during RL*: Another category of research involves the integration of previous demonstrations during the RL exploration by seamlessly incorporating this experience into the replay buffer. This approach is exemplified in [28], where policy gradient updates are enriched with demonstration data in a weighted manner. This innovative strategy enhances the learning process by leveraging the knowledge encapsulated in expert demonstrations.

Furthermore, researchers have explored the use of offline RL paradigms to amplify sample efficiency in several approaches [29, 30, 31]. Despite these advancements, the application of offline reinforcement learning in real-world agile platforms remains a relatively uncharted territory [27].

While fine-tuning methods have demonstrated success across various robot platforms, particularly in tasks such as dexterous manipulation and object-goal navigation, our work focuses on addressing the unique challenges associated with developing visuomotor policies tailored for quadrotor platforms.

III. METHODOLOGY

A. Problem Formulation

The drone racing task can be formulated as an optimization problem where the objective is to minimize the time required to navigate through a predefined sequence of gates, as illustrated in Fig. 3. The drone perceives the environment solely through a single RGB camera, and the learned policy network utilizes egocentric vision input to generate control commands.

Our goal is to train an end-to-end policy capable of completing the race track using solely visual information. The policy $\pi(\mathbf{o}_p)$ directly outputs control commands based on perceptual observations \mathbf{o}_p from the camera. The output of the policy is the CTBR control command $\mathbf{a} = [c, \omega_x, \omega_y, \omega_z]$, where c represents collective thrust, and ω denotes the bodyrates.

B. Quadrotor Dynamics for Policy Training

The quadrotor is assumed to be a 6 degree-of-freedom rigid body of mass m and diagonal moment of inertia matrix $\mathbf{J} = \text{diag}(J_x, J_y, J_z)$. Furthermore, the rotational speeds of the four propellers Ω_i are modeled as a first-order system with a time constant k_{mot} where the commanded motor speeds Ω_{cmd} are

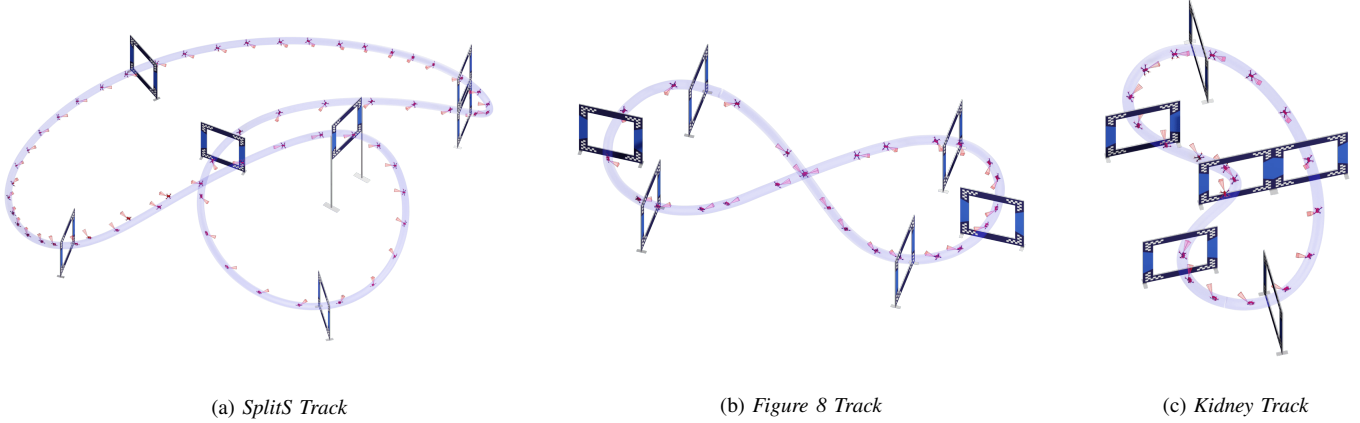


Fig. 3: The efficacy of your acquired visuomotor policies is demonstrated through validation in the context of autonomous drone racing. The assessed policies rely solely on a time sequence of visual information control a quadrotor to navigate on three diverse race tracks, each characterized by varying levels of complexity. Despite differences in complexity, these tracks maintain a consistent size, spanning widths from 8 meters to 16 meters.

the input. World \mathcal{W} and Body \mathcal{B} frames are defined with an orthonormal basis i.e. $\{\mathbf{x}_{\mathcal{W}}, \mathbf{y}_{\mathcal{W}}, \mathbf{z}_{\mathcal{W}}\}$. The frame \mathcal{B} is located at the center of mass of the quadrotor. The state space is thus 17-dimensional and its dynamics can be written as:

$$\dot{\mathbf{x}} = \begin{bmatrix} \dot{\mathbf{p}}_{\mathcal{W}\mathcal{B}} \\ \dot{\mathbf{q}}_{\mathcal{W}\mathcal{B}} \\ \dot{\mathbf{v}}_{\mathcal{W}} \\ \dot{\boldsymbol{\omega}}_{\mathcal{B}} \\ \dot{\boldsymbol{\Omega}} \end{bmatrix} = \begin{bmatrix} \mathbf{v}_{\mathcal{W}} \\ \mathbf{q}_{\mathcal{W}\mathcal{B}} \cdot \begin{bmatrix} 0 & \boldsymbol{\omega}_{\mathcal{B}}/2 \end{bmatrix}^{\top} \\ \frac{1}{m} (\mathbf{q}_{\mathcal{W}\mathcal{B}} \odot (\mathbf{f}_{\text{prop}} + \mathbf{f}_{\text{drag}})) + \mathbf{g}_{\mathcal{W}} \\ \mathbf{J}^{-1} (\boldsymbol{\tau}_{\text{prop}} - \boldsymbol{\omega}_{\mathcal{B}} \times \mathbf{J} \boldsymbol{\omega}_{\mathcal{B}}) \\ \frac{1}{k_{\text{mot}}} (\boldsymbol{\Omega}_{\text{cmd}} - \boldsymbol{\Omega}) \end{bmatrix}, \quad (1)$$

where $\mathbf{g}_{\mathcal{W}} = [0, 0, -9.81 \text{ m/s}^2]^{\top}$ denotes earth's gravity, \mathbf{f}_{prop} , $\boldsymbol{\tau}_{\text{prop}}$ are the collective force and the torque produced by the propellers, and \mathbf{f}_{drag} is a linear drag term. The quantities are calculated as follows:

$$\mathbf{f}_{\text{prop}} = \sum_i \mathbf{f}_i, \quad \boldsymbol{\tau}_{\text{prop}} = \sum_i \boldsymbol{\tau}_i + \mathbf{r}_{\text{p},i} \times \mathbf{f}_i, \quad (2)$$

$$\mathbf{f}_{\text{drag}} = - \begin{bmatrix} k_{vx} v_{\mathcal{B},x} & k_{vy} v_{\mathcal{B},y} & k_{vz} v_{\mathcal{B},z} \end{bmatrix}^{\top}, \quad (3)$$

where $\mathbf{r}_{\text{p},i}$ is the location of propeller i expressed in the body frame, \mathbf{f}_i , $\boldsymbol{\tau}_i$ are the forces and torques generated by the i -th propeller, and (k_{vx}, k_{vy}, k_{vz}) [32, 33] are linear drag coefficients.

C. Actor-Critic Reinforcement Learning

The Actor-Critic method is a widely-used approach in reinforcement learning (RL) that combines the advantages of both value-based and policy-based methods [34, 19]. It consists of two main components: the Actor and the Critic. The key idea is to simultaneously learn a state-value function $V_{\omega}(s)$ and learn a policy function π_{θ} , where the value function (Critic) and policy (Actor) are parameterized by ω and θ separately. The policy is updated via the policy gradient theorem [35],

$$\nabla_{\theta} J(\pi_{\theta}) = \frac{1}{N} \sum_{i=1}^N \sum_{k=1}^T \nabla_{\theta} \log \pi_{\theta}(a_k^i | s_k^i) A_{\omega}(s_k^i, a_k^i) \quad (4)$$

where $A(s_k, a_k) = r(s_k, a_k) + \gamma V_{\omega}(s_{k+1}) - V_{\omega}(s_k)$ is the advantage function. Here, $s_k \in \mathcal{S}$ is the observation, $a_k \in \mathcal{A}$ is the action. In a standard actor-critic method, the policy is a stochastic representation where the mean is $a_k = f_{\theta}(s_k)$ a function approximator, such as a feedforward neural network. This way, the actor's policy guides the selection of actions, which is updated through interactions with the environment. Simultaneously, the critic evaluates the chosen actions, estimating the value function $V(s)$ to provide feedback on expected cumulative rewards. The training process involves iteratively refining the actor and critic parameters based on observed rewards and anticipated future outcomes. The update of the policy is achieved through the application of the policy gradient theorem:

$$\mathcal{L}^{PG}(\theta) = \hat{\mathbb{E}}_t [\nabla_{\theta} J(\pi_{\theta})] \quad (5)$$

In our work, we use the Proximal Policy Gradient (PPO) [19] as the RL algorithm. The policy gradient could be written as:

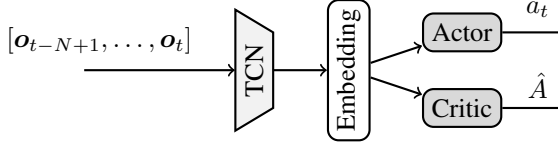
$$\mathcal{L}(\theta) = \hat{\mathbb{E}}_t \left[\min(r_t(\theta) \hat{A}_t, \text{clip}(r_t(\theta), 1 - \epsilon, 1 + \epsilon) \hat{A}_t) \right] \quad (6)$$

Here $r_t(\theta)$ denotes the probability ratio of $\frac{\pi_{\theta}(a_t | s_t)}{\pi_{\theta_{\text{old}}}(a_t | s_t)}$, and ϵ sets a clip upper bound to constrain the policy update rate. Typically, the actor and critic functions use the same input, as shown in Fig. 4 (a). In vision-based Reinforcement Learning (RL), it has been demonstrated that employing an asymmetric actor-critic setup is advantageous, as illustrated in Fig. 4 (b). The concept involves integrating the critic function with more privileged information, such as the robot state s . By appending additional information, the efficiency, and performance of RL training can be significantly improved.

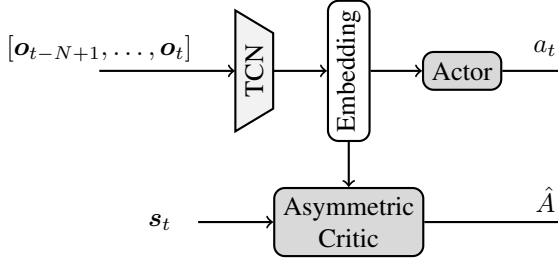
D. State-based Teacher Policy Training

The teacher policy π_{teacher} processes state observations $\mathbf{s} = [\mathbf{p}, \tilde{\mathbf{R}}, \mathbf{v}, \boldsymbol{\omega}, \mathbf{i}, \mathbf{d}]$, where $\mathbf{p} \in \mathbb{R}^3$ represents the drone's position, $\tilde{\mathbf{R}} \in \mathbb{R}^6$ is a vector comprising the first two columns

of $\mathcal{R}_{\mathcal{WB}}$ [36], $\mathbf{v} \in \mathbb{R}^3$ and $\boldsymbol{\omega} \in \mathbb{R}^3$ denote the linear and angular velocity of the drone, and $\mathbf{d} \in \mathbb{R}^3$ represents the position of the next gate center relative to the current drone position. At each timestep, the policy receives an observation from the environment that includes both the current state \mathbf{s}_t of the robot and its relative position to the upcoming waypoint to be traversed. The training of the teacher policy employs



(a) Symmetric Actor-Critic configuration.



(b) Asymmetric Actor-Critic configuration.

Fig. 4: In our experiments, we explore various Actor-Critic reinforcement learning configurations. In configuration (a), a time series of visual observations is initially concatenated and processed through a Temporal Convolution Network (TCN [37]). The resulting temporal embedding is utilized for both actor and critic functions concurrently. On the other hand, configuration (b) represents an asymmetric setting. In addition to the temporal embedding from TCN, the critic function incorporates robot state information as a network input. Leveraging more privileged information in this asymmetric setup has the potential to enhance learning efficiency.

a model-free reinforcement learning approach with PPO. We have customized the reward formulation, drawing inspiration from adjustments proposed in [38, 39]. The reward at time t , denoted as r_t , is defined as the sum of various components:

$$r_t = r_t^{\text{prog}} + r_t^{\text{perc}} + r_t^{\text{act}} + r_t^{\text{br}} + r_t^{\text{pass}} + r_t^{\text{crash}} \quad (7)$$

where r_t^{prog} encourages progress towards the next gate to be passed [40], r_t^{perc} encodes perception awareness by adjusting the quadrotor’s attitude such that the optical axis of its camera points towards the next gate’s center, r_t^{act} penalizes action changes from the last time step, r_t^{br} penalizes bodyrates and consequently reduces motion blur, r_t^{pass} is a binary reward that is active when the robot successfully passes the next gate, r_t^{crash} is a binary penalty that is only active when a collision happens, which also ends the episode. The reward components

are formulated as follows:

$$\begin{aligned} r_t^{\text{prog}} &= \lambda_1 (d_{\text{Gate}}(t-1) - d_{\text{Gate}}(t)) \\ r_t^{\text{perc}} &= \lambda_2 \exp(\lambda_3 \cdot \delta_{\text{cam}}^4) \\ r_t^{\text{act}} &= -\lambda_3 \|a_t - a_{t-1}\| \\ r_t^{\text{br}} &= -\lambda_4 \|\boldsymbol{\omega}_t\| \\ r_t^{\text{pass}} &= c_1, \quad \text{if robot passes the next gate} \\ r_t^{\text{crash}} &= -c_2, \quad \text{if robot crashes (gates, ground)} \end{aligned} \quad (8)$$

Here $d_{\text{Gate}}(t)$ denotes the distance from the robot’s center of mass to the center of the next gate to pass, δ_{cam} is the angle between the camera’s optical axis and the direction towards the center of the next gate. \mathbf{a} represents the control command, and $\boldsymbol{\omega}$ the bodyrate. $\lambda_1, \lambda_2, \lambda_3, \lambda_4, c_1, c_2$ are different positive hyperparameters.

E. Imitation Learning using Visual Input

The goal of IL is to learn a behavior policy π_{student} from the expert π_{teacher} . The vision-based student policy takes a sequence (history length N timesteps) of perceptual observations $[o_{t-N+1}, \dots, o_t]$ as input. Then we use a Temporal Convolutional Network (TCN [37]) to encode the series of vision embeddings from \mathcal{I} or corners \mathcal{C} . Then the output features from two TCNs are concatenated and fed into a two-layer MLP, which outputs the actions. The supervision loss is formulated as \mathcal{L}_A (action error), which is the mean square error between the outputs of the teacher policy and the student policy.

$$\mathcal{L}_A = \|\pi_{\text{student}}(o_t) - \pi_{\text{teacher}}(s_t)\| \quad (9)$$

To acquire an imitation learning policy, one can employ either (i) Behavior Cloning (BC) or (ii) DAgger [1].

In the case of BC, the state-based teacher policy is executed for a fixed number of steps, generating a dataset that encompasses corresponding perceptual observations and action outputs. In contrast, DAgger involves iteratively training the student policy by executing the learned student policy with a gradually increasing probability over time. The data collected from rolling out the student actions include a balanced representation of both positive and negative experiences. This approach results in improved performance compared to traditional BC, contributing to more effective learning.

F. Policy Fine-tuning through RL

At this stage, we initiate the fine-tuning process using the pre-trained student policy as the starting point in RL. However, a straightforward plug-and-play approach may not yield optimal results due to two key challenges: (i) the critic function requires interactions to adapt the pre-trained actor, necessitating a “warm-up” process. Otherwise, the critic will provide poor value estimates that can impact the actor’s gradient updates, as depicted in Eq. 4. (ii) During the initial training phase, policy update steps should be kept relatively small to prevent catastrophic forgetting resulting from sudden, large updates. While a fixed learning rate schedule based on training iterations could address this issue, we propose that a

performance-based scheduling approach is more suitable for policy fine-tuning. The exploration and learning rates should dynamically depend on the agents’ performance rather than being solely determined by the number of iterations.

Our fine-tuning strategy can be summarized as follows: First, we execute the pre-trained policy and record the collected reward as r_{init} . Subsequently, we set the learning rate for the policy network with LR_{π} and initialize the learning rate for the value function with LR_V . Following this, we continue training the standard Actor-Critic RL, and at each N step, we evaluate the policy and collect the sum of rewards, denoted as r_{rollout} . We then model the policy improvement using the ratio $\alpha = \frac{r_{\text{rollout}}}{r_{\text{init}}}$ and update (i) the learning rates of the actor and critic function and (ii) the PPO clip range in Eq. 6:

$$LR_{\pi} = \min(LR_{\pi} + \max(\alpha - 1, 0) * c_V, LR_{\pi\text{max}}) \quad (10)$$

$$LR_V = \max(LR_V - \max(\alpha - 1, 0) * c_{\pi}, LR_{V\text{min}}) \quad (11)$$

$$\epsilon = \min(\epsilon + \max(\alpha - 1, 0) * c_{\epsilon}, \epsilon_{\text{max}}) \quad (12)$$

Here $c_V, c_{\pi}, c_{\epsilon}$ are positive constants controlling the update size of the learning rate. By relying on a performance-dependent update schedule rather than one based on the number of interactions, we aim to enhance the sample efficiency of the data exploration.

During training, we initialize by freezing the actor and exclusively training the critic for N (usually 100K) iterations, laying the foundation for value network training. Subsequently, we unfreeze both the value and policy networks to initiate performance-adaptive policy fine-tuning. As the interaction increases, the value function updates more slowly as the trajectory converges to a consistent solution. Simultaneously, the policy network benefits from an increasing learning rate and a smaller clip range, promoting exploration and thereby enhancing performance further. It’s worth noting that we apply upper and lower bounds, namely $LR_{\pi\text{max}}, LR_{V\text{min}}, \epsilon_{\text{max}}$, to the policy networks and value function’s update rate to ensure stable training convergence. For a detailed analysis of the parameters and visualization of the learning rate curve during training, we refer the readers to the supplementary materials.

IV. EXPERIMENTS AND RESULTS

A. Experimental Setup

We validate our approach on three different race tracks, as shown in Fig. 3, namely the “*SplitS*”, “*Figure 8*”, and “*Kidney*” tracks. During the evaluation, we roll out the policy until it completes 10 laps. Otherwise, for 3000 simulation time steps, i.e., 50s. For each policy to be evaluated, we run 100 experiments with different starting positions. For the sake of a fair comparison, we use the same set of starting positions for all policies. These positions are uniformly sampled from the 3D box with a side length of 1 meter centered at the nominal starting position for the racing track.

Here, we employ three distinct evaluation metrics: success rate (SR%), gate passing error (Error [m]), and lap time (Lap Time [s]). The success rate is defined as the number of completed laps divided by the total trials. Gate pass error

indicates the distance norm between the drone’s position and the gate center when passing the gate. Lap time illustrates the time required to complete a full race track (fly through all the gates).

B. Training Configurations

For state-based teacher training, we employ a policy network consisting of a two-layer MLP, each layer containing 256 neurons, with a final layer outputting a 4-dimensional vector using a *tanh* activation function.

In imitation learning, a 3-layer Temporal Convolutional Network (TCN) is utilized to encode the 32 timestamps of perceptual inputs. The length of the temporal embedding is 128, followed by another two-layer MLP to output the control command. For imitation learning, we employ a batch size of 512, and convergence typically occurs after collecting 5M data samples over approximately 100 epochs. We incorporate a linear decay in the learning rate, starting at 1e-3 and decreasing to 1e-5 at 50 epochs, remaining unchanged for the remainder of the training process.

For more details on the reward and fine-tuning hyperparameters, we kindly refer the readers to the supplementary materials.

C. Hardware Configurations

We deploy our approach in the real world using a high-performance racing drone with a maximum thrust-to-weight ratio (TWR) of 5.78. However, for our experiments, we have limited the TWR to 2.7. We use a modification of the *Agilicious* platform [42] for the real-world deployment. We have replaced the onboard computer with an RF receiver, which is connected directly to the flight controller¹ and takes care of parsing the collective thrust and bodyrate commands from the computer. Additionally, we also mount an ultra-low latency camera feed sender, which sends the live video stream to the base computer. This configuration is similar to the one used by professional drone racing pilots.

D. Detailed Analysis

In this subsection, we conduct a series of experiments and ablation studies to address various research questions, aiming to demonstrate detailed insights into our proposed approach.

How are different IL approaches applicable for vision-based flight? Employing the state-based teacher policy, we utilize two IL approaches: DAgger [1] and behavior cloning. Our visuomotor policy employs a TCN followed by a two-layer MLP to process a history of visual embeddings and generate control commands. To accommodate the race track and our 60Hz control frequency, we adopt a history length of 32 timestamps (approximately 5 seconds). To evaluate the performance of our approach, we conduct IL experiments with two categories of visual input: (i) implicitly learned from ResNet [41] and (ii) task-relevant gate corners in the pixel frame.

¹<https://www.betaflight.com>

TABLE I: This table displays the evaluation results of vision-based policies utilizing both implicitly learned representations, specifically a common ResNet50 [41], and explicit task representations—the pixel information of the gate corners—across three different racing tracks. While behavior cloning (BC) and reinforcement learning (RL) from scratch fail to complete the task, DAgger [1], and our approach both achieve a 100% success rate. Our method clearly exhibits the highest-performing policy in terms of lap time and average gate passing errors.

Visual Input	Category	Methods	Race Tracks								
			Figure 8			SplitS			Kidney		
			SR%	Error [m]	Lap Time [s]	SR%	Error [m]	Lap Time [s]	SR%	Error [m]	Lap Time [s]
Pixel	Direct	DAgger [1]	100	0.18	4.60±0.23	100	0.27	7.96±0.17	100	0.18	5.41±0.18
		BC	0	-	-	0	-	-	0	-	-
		RL [19]	0	-	-	0	-	-	0	-	-
	Finetuning	Ours	100	0.16	4.27±0.21	100	0.22	7.71±0.32	100	0.17	4.81±0.17
Corners	Direct	DAgger [1]	100	0.19	4.82±0.17	100	0.24	7.94±0.24	100	0.15	5.42±0.16
		BC	0	-	-	0	-	-	0	-	-
		RL [19]	0	-	-	0	-	-	0	-	-
	Finetuning	PIRLNav [27]	17	0.56	6.12±0.32	0	-	-	14	0.67	6.42±0.41
		Ours	100	0.20	4.54±0.13	100	0.22	7.68±0.10	100	0.15	5.18±0.08

In (i), we employ a pre-trained ResNet50 [41] network on ImageNet [43] to produce implicit embeddings. The ResNet outputs a 128-dimensional embedding. Hence, the input of the TCN network corresponds to the history of the embeddings, which is 32×128 .

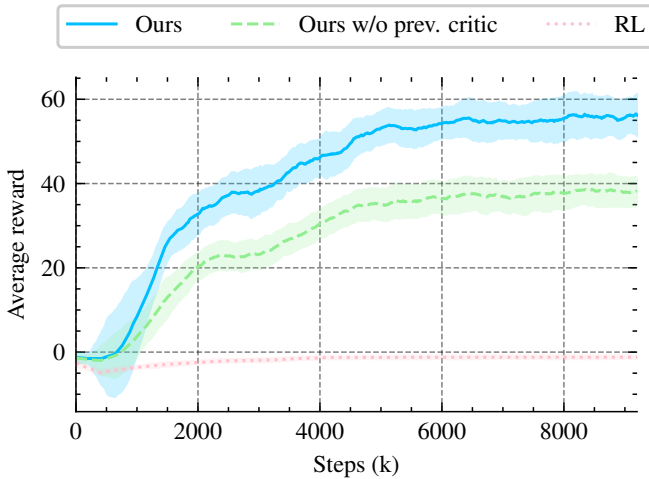


Fig. 5: Comparing rewards across different RL configurations for the SplitS track using ResNet embedding, we find that utilizing an asymmetric critic makes the learning process more efficient. As a result, we have selected this configuration as the default setting for our other experiments.

For (ii) task-relevant visual input, we utilize the *normalized pixel coordinates* of all gate corners projected in the camera view. We model gate corners based on the gate detection system presented in [7]. To simulate real-world scenarios, we introduce factors such as gate scales, pixel position noise (10 pixels in both (u, v) in a 1280×760 image frame), and a 10% random missing probability for each corner at each frame to mimic data detection failures. In our work, we utilize the habitat sim simulator [44] to enable fast real-time rendering.

After projection, we sort the gate corner pixels by their u coordinates, and we model corners out of the image view as $(-1, -1)$. The observation space for each track is $32 \times N_{\text{gate}} \times N_{\text{corner}} \times 2$, where N_{gate} is the number of gates per track, and N_{corner} represents the corner numbers per gate. Even for tracks with 6 gates, the observation space remains $32 \times 6 \times 4 \times 2 = 1536$. Detailed simulation visualizations for both inputs are

available in the supplementary video. Consequently, in both cases, the policy needs to effectively handle high-dimensional egocentric visual input.

We execute various IL approaches using the same number of 10M steps until training convergence. The results are illustrated in Table I. From this table, it is evident that the DAgger approach demonstrates high success rates for all racing tracks, with both implicit and explicit visual inputs. In contrast, the BC approach struggles, particularly in navigating through the first gate. This underscores the complexity of vision-based quadrotor flight, as high update rates of control commands pose a significant challenge with only perceptual input.

How does the training configuration affect the performance of visuomotor policy?

After the imitation learning stages, our visuomotor policy undergoes fine-tuning using two different setups, as illustrated by the blue and green curves in Fig.5. Here, we examine how the critic configurations, as demonstrated in Fig.4, can impact policy fine-tuning. As depicted in Fig. 5, RL fine-tuning with an asymmetric critic function achieves the highest reward within the same budget. Fine-tuning with the symmetric critic function also shows a considerable improvement compared to RL from scratch. This observation leads to two conclusions: (i) Our fine-tuning strategy significantly enhances learning efficiency, even for tasks where RL from scratch is ineffective. (ii) In vision-based RL, employing an asymmetric critic function with more privileged state information can boost policy performance. As a result, we opt to use the asymmetric setup for the subsequent experiments.

How does our approach compare to the baselines?

To demonstrate the effectiveness of our visuomotor policy learning approach, we select several baseline policies: (i) RL from scratch, (ii) DAgger from scratch, and (iii) the PIRLNav approach [27]. PIRLNav was originally designed for an object-goal navigation task where the agent needs to output discrete high-level commands such as “move forward” or “turn right.” The algorithm utilizes a BC policy and then undergoes RL fine-tuning with a fixed learning rate schedule.

To benchmark these algorithms, we train the direct approaches (IL and RL from scratch) for 10M steps. For fine-tuning approaches, we conduct 5M steps for IL policy training

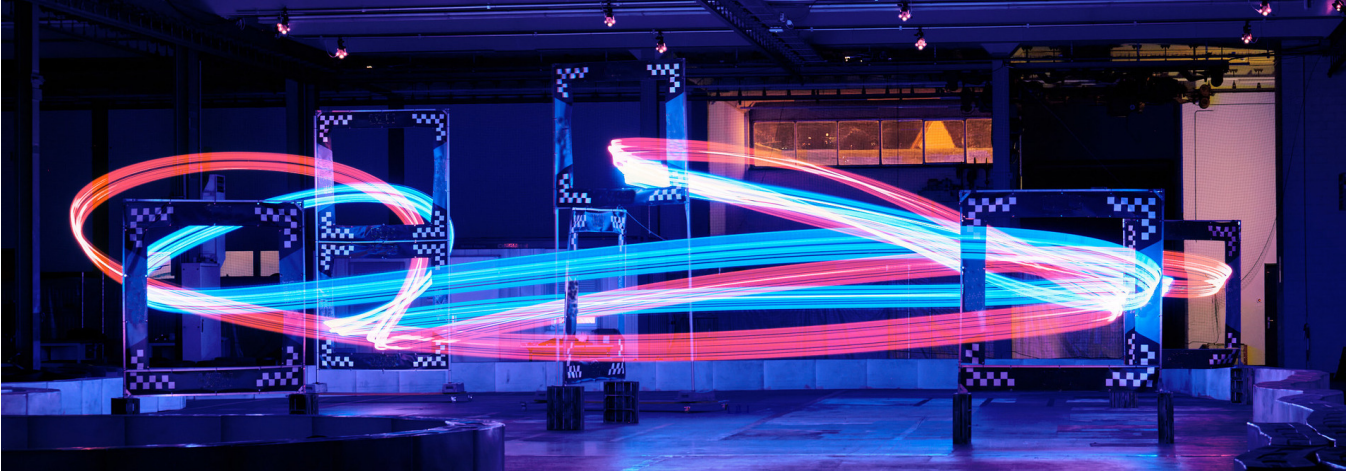


Fig. 6: Long exposure image of real-world flights. The blue trajectory represents our fine-tuned policy, while the red one corresponds to the imitation policy. Our fine-tuned policy follows a tighter trajectory, demonstrating superior performance.

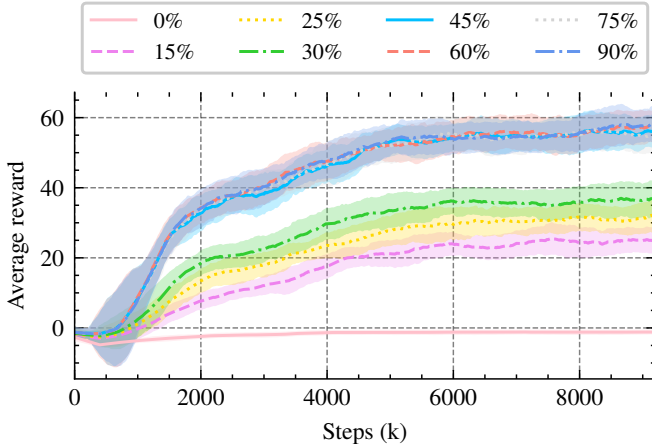


Fig. 7: Rewards visualization for the SplitS track using policies from pixels with ResNet. By varying percentages (from 10% to 90%) of DAGger policies in fine-tuning using our proposed approach. Our approach reveals substantial benefits, even with 15% of data samples for policy training.

and 5M steps for RL fine-tuning. We maintain the same network architecture and training parameters for all three tracks, by utilizing both explicit and implicit visual inputs. The final results are presented in Table I.

Firstly, it is noteworthy that the direct RL from corners or pixels achieves a 0% success rate in all three tracks. This once again underscores the difficulty of RL exploration in high-dimensional time series without bootstrapping. Next, we compare our method against (i) DAGger and (ii) PIRLNav. For (i), both our approach and DAGger ultimately achieve a 100% success rate. While both demonstrate considerable robustness, our method exhibits superior performance in terms of lap times and gate-passing errors. Across all configurations and racing tracks, utilizing two different types of vision input, our fine-tuned policies consistently exhibit faster lap times compared to imitation learning (IL) under the same data sample budget.

As for (ii), BC fine-tuning with a fixed schedule exhibits weaker robustness (lower SR%) compared to our approach. On

a long-range track like *SplitS*, BC fine-tuning using PIRLNav cannot even achieve successful performance. On the shorter track such as Fig 8, RL can fine-tune the policy to a relatively low success rate (17%), although its performance falls significantly below that of our fine-tuning approach (100%). Given the suboptimal performance of corner-based policies, especially on the *SplitS* track, we choose not to delve further into investigating the effects of BC fine-tuning strategies.

The comparison in (ii) raises an interesting question. One major difference between our approach and [27] lies in the performance of the imitation policy for bootstrapping. Therefore, it is natural to pose the following question:

How does our approach fine-tune the pre-trained policies with different performance? To address this question, we test different percentages (ranging from 10% to 90%) of the DAGger policies and fine-tune them using our proposed approach. The detailed training plots are illustrated in Fig. 7. Notably, even with only 15% (1.5M) of the data samples used for policy training, we observe significant benefits (> 20 rewards) compared to training from scratch (< 0 rewards). Furthermore, as we allocate a larger portion of data samples for pre-training, our strategy demonstrates the ability to enhance performance to a higher level. However, we observe that the improvement plateaus and converges (at around 60) at the same level after surpassing 45% pretraining, as the DAGger training has already converged at 40M samples.

Using this conclusion, it is not hard to infer that given a fixed data sample budget, there should be an optimal ratio range so that pre-training improves the performance of the resulting policies. This leads to our next question:

Given a fixed sample budget, how does the pre-training ratio affect policies' performance? As depicted in Fig. 8, while fixing the total sample budget at 10M and varying the pre-training partition, we visualize the deployment reward of the resulting policies. It is evident that at 60%, there is a peak (> 100) in the curve representing the best performance. The plot indicates that by using an appropriate amount of data, the

TABLE II: Real-world performance comparison between imitation learning (IL) and our fine-tuned approach for two types of input representations (Corners and Images) across different race tracks. Our fine-tuned policy consistently outperforms IL, showcasing, reduced errors, and faster lap times. Furthermore, our approach consistently demonstrates superior performance compared to DAgger when utilizing the same 1M sample budget.

Input	Methods	Race Tracks								
		Figure 8			SplitS			Kidney		
		SR%	Error [m]	Lap Time [s]	SR%	Error [m]	Lap Time(s)	SR%	Error [m]	Lap Time [s]
Corners	IL	100%	0.49	4.85±0.45	100%	0.55	8.18±0.54	100%	0.37	5.76±0.28
	Ours	100%	0.26	4.60±0.46	100%	0.29	7.83±0.35	100%	0.29	5.22±0.31
Images	IL	100%	0.35	4.69±0.48	100%	0.48	8.06±0.52	100%	0.35	5.45±0.33
	Ours	100%	0.27	4.30±0.42	100%	0.31	7.67±0.42	100%	0.18	4.93±0.31

performance can easily surpass policies trained solely from IL (around 86).

Then the next question moves to: **How does the performance transfer to the real-world scenarios?** To showcase the effects of policy improvement, we validate our policy in real-world scenarios. To minimize uncertainty arising from sensor mismatch, the validation is conducted through Hardware-in-the-Loop (HIL) simulation. A VICON motion capture system is utilized to generate corresponding perceptual input via rendering or gate corner projections. For both perceptual inputs, we employ the 5M pre-trained and 5M fine-tuned (50%) policy, benchmarking against the 10M DAgger policy. The results are presented in Table II. For detailed footage and onboard visual inputs, we refer the readers to the supplementary materials.

All policies were tested by completing 10 consecutive racing laps. The success rate, gate passing error, and average lap times were recorded. In all the race tracks, our fine-tuned policies achieve faster lap times and smaller gate errors. The experiments successfully demonstrate that our policy enhancement can be effectively transferred into a real-world vision-based quadrotor. Using real-world data, we visualize the trajectory

and the velocity profile for both flights and try to answer the question:

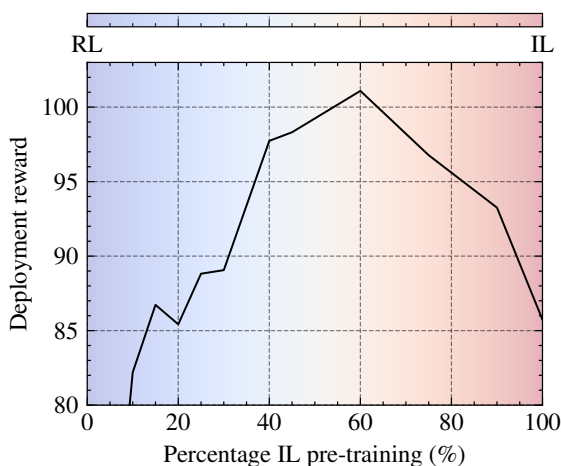


Fig. 8: By utilizing a fixed sample budget, we vary the percentage of the associated imitation learning (IL) policy for vision-based SplitS track training using ResNet. We demonstrate the ability to achieve a local maximum in deployment reward by employing 60% IL pretraining and 40% RL fine-tuning.

How does our approach affect the policy performance?

To understand how our fine-tuning strategy improves the policy the real-world trajectories using ResNet from both approaches, a top view of the trajectory is shown in Fig. 9. It becomes apparent that fine-tuning the policy results in a tighter trajectory, consequently producing a higher peak velocity. For example, in the part of the track containing the challenging *SplitS* maneuver (bottom to bottom-left corner of Fig. 9, one can notice how the RL-fine tuned trajectory makes a tighter turn and then a longer straight, a maneuver that emerges from RL and that allows the agent to compromise less in overall speed. This is one example of how RL fine-tuning guides the policy to re-discover new maneuvers that enable higher velocity and, consequently, faster flight. Such improvements are not attainable through imitation learning alone.

V. DISCUSSION

In this work, we introduced a novel approach by fusing the strengths of Reinforcement Learning (RL) and Imitation Learning (IL) for vision-based agile quadrotor flight, specifically focusing on autonomous drone racing. By leveraging the advantages of both RL and IL, our approach demonstrates significant improvements in performance and robustness compared to using either method in isolation.

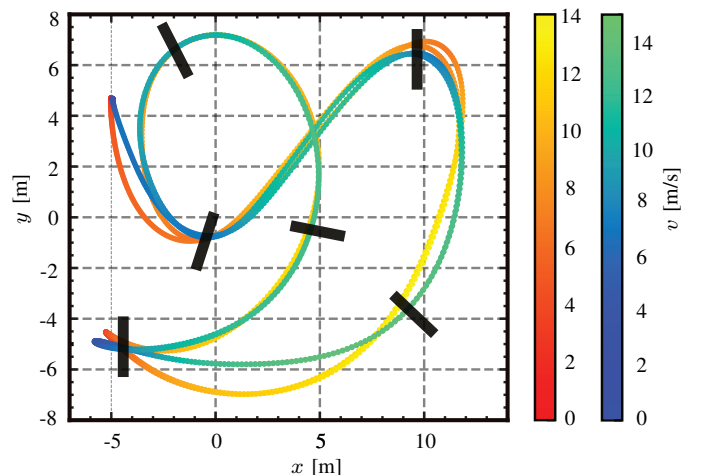


Fig. 9: Comparison of real-world trajectories on the SplitS track: ours (green) achieves 7.67s lap time, while DAgger's (orange) is 8.06s. The black blocks are the corresponding gates. On the right side, the velocity profiles for different policies are illustrated. Utilizing the same data budget, our approach enables a tighter trajectory for higher peak speed (blue color bar) and faster flight.

One key finding of this study is the superior performance of the RL fine-tuned policy over the IL policy in terms of lap time and trajectory execution. We demonstrated that, under a fixed number of sample budgets, there exists a maximum reward policy by synergizing IL and RL. Through a series of experiments in simulated and real-world environments, the RL fine-tuned policy consistently outperformed the IL policy, showcasing the ability to execute tighter trajectories and achieve faster flight speeds. This performance advantage is crucial in drone racing competitions, where even a small improvement in lap time can make a significant difference. By combining RL and IL, our approach overcomes these limitations and presents a more effective training framework for vision-based agile flight tasks.

The proposed training framework consists of three stages: (i) Initial training of a teacher policy with privileged state information, (ii) distillation of this policy into a student policy using IL, and (iii) performance-constrained adaptive RL fine-tuning.

We prove our approach to be successful in achieving superior performance and robustness in navigating a quadrotor through a racing course using only visual information without explicit state estimation. This innovative approach not only enhances the efficiency of learning visuomotor policies but also highlights the potential for further advancements in autonomous drone racing and other agile-flight applications.

In conclusion, the integration of RL and IL in vision-based agile flight tasks presents a promising avenue for improving performance, sample efficiency, and robustness in autonomous systems. The findings of this study contribute valuable insights to the field of reinforcement learning and imitation learning, paving the way for future research and development in autonomous drone racing and related domains.

VI. ACKNOWLEDGEMENTS

This work was supported by the European Union’s Horizon Europe Research and Innovation Programme under grant agreement No. 101120732 (AUTOASSESS) and the European Research Council (ERC) under grant agreement No. 864042 (AGILEFLIGHT). The authors especially thank Chunwei Xing and Ismail Geles for their contributions to the design and help with the experiments.

REFERENCES

[1] S. Ross, G. Gordon, and D. Bagnell, “A reduction of imitation learning and structured prediction to no-regret online learning,” in *Proceedings of the Fourteenth International Conference on Artificial Intelligence and Statistics*, pp. 627–635, PMLR, 2011.

[2] A. Loquercio, E. Kaufmann, R. Ranftl, M. Müller, V. Koltun, and D. Scaramuzza, “Learning high-speed flight in the wild,” *Science Robotics*, vol. 6, no. 59, p. eabg5810, 2021.

[3] D. Shah, A. Sridhar, N. Dashora, K. Stachowicz, K. Black, N. Hirose, and S. Levine, “ViNT: A foundation

model for visual navigation,” in *7th Annual Conference on Robot Learning*, 2023.

[4] C. Chi, S. Feng, Y. Du, Z. Xu, E. Cousineau, B. Burchfiel, and S. Song, “Diffusion policy: Visuomotor policy learning via action diffusion,” in *Proceedings of Robotics: Science and Systems (RSS)*, 2023.

[5] S. Levine, C. Finn, T. Darrell, and P. Abbeel, “End-to-end training of deep visuomotor policies,” *The Journal of Machine Learning Research*, 2016.

[6] Z. Zhuang, Z. Fu, J. Wang, C. Atkeson, S. Schwertfeger, C. Finn, and H. Zhao, “Robot parkour learning,” *Conference on Robot Learning (CoRL)*, 2023.

[7] E. Kaufmann, L. Bauersfeld, A. Loquercio, M. Müller, V. Koltun, and D. Scaramuzza, “Champion-level drone racing using deep reinforcement learning,” *Nature*, vol. 620, pp. 982–987, Aug 2023.

[8] E. Kaufmann, A. Loquercio, R. Ranftl, M. Müller, V. Koltun, and D. Scaramuzza, “Deep drone acrobatics,” in *Proceedings of Robotics: Science and Systems*, (Corvallis, Oregon, USA), July 2020.

[9] Y. Song, A. Romero, M. Mueller, V. Koltun, and D. Scaramuzza, “Reaching the limit in autonomous racing: Optimal control versus reinforcement learning,” *Science Robotics*, p. adg1462, 2023.

[10] Y. Ji, G. B. Margolis, and P. Agrawal, “Dribblebot: Dynamic legged manipulation in the wild,” *IEEE International Conference on Robotics and Automation (ICRA)*, 2023.

[11] Z. Fu, T. Z. Zhao, and C. Finn, “Mobile aloha: Learning bimanual mobile manipulation with low-cost whole-body teleoperation,” *arXiv preprint arXiv:2401.02117*, 2024.

[12] J. Xing, L. Bauersfeld, Y. Song, C. Xing, and D. Scaramuzza, “Contrastive learning for enhancing robust scene transfer in vision-based agile flight,” in *2024 IEEE international conference on robotics and automation (ICRA)*, IEEE, 2024.

[13] A. Agarwal, A. Kumar, J. Malik, and D. Pathak, “Legged locomotion in challenging terrains using egocentric vision,” in *Conference on Robot Learning*, pp. 403–415, PMLR, 2022.

[14] A. Rosinol, M. Abate, Y. Chang, and L. Carlone, “Kimera: an open-source library for real-time metric-semantic localization and mapping,” in *IEEE Intl. Conf. on Robotics and Automation (ICRA)*, 2020.

[15] B. Sun, J. Xing, H. Blum, R. Siegwart, and C. Cadena, “See yourself in others: Attending multiple tasks for own failure detection,” in *2022 International Conference on Robotics and Automation (ICRA)*, pp. 8409–8416, IEEE, 2022.

[16] C. Campos, R. Elvira, J. J. G. Rodríguez, J. M. Montiel, and J. D. Tardós, “Orb-slam3: An accurate open-source library for visual, visual-inertial, and multimap slam,” *IEEE Transactions on Robotics*, 2021.

[17] C. Forster, M. Pizzoli, and D. Scaramuzza, “Svo: Fast semi-direct monocular visual odometry,” *2014 IEEE International Conference on Robotics and Automation*

- (ICRA), pp. 15–22, 2014.
- [18] J. Xing, G. Cioffi, J. Hidalgo-Carrió, and D. Scaramuzza, “Autonomous power line inspection with drones via perception-aware mpc,” in *2023 IEEE/RSJ International Conference on Intelligent Robots and Systems (IROS)*, pp. 1086–1093, IEEE, 2023.
- [19] J. Schulman, F. Wolski, P. Dhariwal, A. Radford, and O. Klimov, “Proximal policy optimization algorithms,” *arXiv preprint arXiv:1707.06347*, 2017.
- [20] F. Torabi, G. Warnell, and P. Stone, “Behavioral cloning from observation,” in *IJCAI*, pp. 4950–4957, 2018.
- [21] R. Rafailov, K. B. Hatch, V. Kolev, J. D. Martin, M. Phielipp, and C. Finn, “Moto: Offline to online fine-tuning for model-based reinforcement learning,” in *Conference on Robot Learning (CoRL)*, 2023.
- [22] L. Pinto, M. Andrychowicz, P. Welinder, W. Zaremba, and P. Abbeel, “Asymmetric actor critic for image-based robot learning,” in *Proceedings of Robotics: Science and Systems*, July 2017.
- [23] M. Laskin, A. Srinivas, and P. Abbeel, “Curl: Contrastive unsupervised representations for reinforcement learning,” in *ICML*, 2020.
- [24] S. Schaal, “Learning from demonstration,” *Advances in neural information processing systems*, vol. 9, 1996.
- [25] B. Baker, I. Akkaya, P. Zhokov, J. Huizinga, J. Tang, A. Ecoffet, B. Houghton, R. Sampedro, and J. Clune, “Video pretraining (vpt): Learning to act by watching unlabeled online videos,” *Advances in Neural Information Processing Systems*, vol. 35, pp. 24639–24654, 2022.
- [26] Y. Zhu, Z. Wang, J. Merel, A. Rusu, T. Erez, S. Cabi, S. Tunyasuvunakool, J. Kramár, R. Hadsell, N. de Freitas, and N. Heess, “Reinforcement and imitation learning for diverse visuomotor skills,” in *Proceedings of Robotics: Science and Systems*, 2018.
- [27] R. Ramrakhya, D. Batra, E. Wijmans, and A. Das, “Pirlnav: Pretraining with imitation and rl finetuning for objectnav,” in *Proceedings of the IEEE/CVF Conference on Computer Vision and Pattern Recognition*, 2023.
- [28] A. Rajeswaran, V. Kumar, A. Gupta, G. Vezzani, J. Schulman, E. Todorov, and S. Levine, “Learning Complex Dexterous Manipulation with Deep Reinforcement Learning and Demonstrations,” in *Proceedings of Robotics: Science and Systems (RSS)*, 2018.
- [29] P. J. Ball, L. Smith, I. Kostrikov, and S. Levine, “Efficient online reinforcement learning with offline data,” *International Conference on Machine Learning 2023*, 2023.
- [30] Q. Li, J. Zhang, D. Ghosh, A. Zhang, and S. Levine, “Accelerating exploration with unlabeled prior data,” *Advances in Neural Information Processing Systems 36 (2023)*, 2023.
- [31] Y. Song, Y. Zhou, A. Sekhari, J. A. Bagnell, A. Krishnamurthy, and W. Sun, “Hybrid rl: Using both offline and online data can make rl efficient,” *ICLR*, 2023.
- [32] F. Furrer, M. Burri, M. Achtelik, and R. Siegwart, “Rotors—a modular gazebo mav simulator framework,” in *Robot Operating System (ROS)*, Springer, 2016.
- [33] M. Faessler, A. Franchi, and D. Scaramuzza, “Differential flatness of quadrotor dynamics subject to rotor drag for accurate tracking of high-speed trajectories,” *RAL*, 2017.
- [34] V. Mnih, A. P. Badia, M. Mirza, A. Graves, T. Lillicrap, T. Harley, D. Silver, and K. Kavukcuoglu, “Asynchronous methods for deep reinforcement learning,” in *International conference on machine learning*, pp. 1928–1937, PMLR, 2016.
- [35] R. S. Sutton, D. McAllester, S. Singh, and Y. Mansour, “Policy gradient methods for reinforcement learning with function approximation,” *Advances in neural information processing systems*, vol. 12, 1999.
- [36] Y. Zhou, C. Barnes, J. Lu, J. Yang, and H. Li, “On the continuity of rotation representations in neural networks,” in *Proceedings of the IEEE/CVF Conference on Computer Vision and Pattern Recognition*, pp. 5745–5753, 2019.
- [37] C. Lea, R. Vidal, A. Reiter, and G. D. Hager, “Temporal convolutional networks: A unified approach to action segmentation,” in *Computer Vision—ECCV 2016 Workshops: Amsterdam, The Netherlands, October 8–10 and 15–16, 2016, Proceedings, Part III 14*, pp. 47–54, Springer, 2016.
- [38] Y. Song, M. Steinweg, E. Kaufmann, and D. Scaramuzza, “Autonomous drone racing with deep reinforcement learning,” in *2021 IEEE/RSJ International Conference on Intelligent Robots and Systems (IROS)*, pp. 1205–1212, IEEE, 2021.
- [39] Y. Song, S. Naji, E. Kaufmann, A. Loquercio, and D. Scaramuzza, “Flightmare: A flexible quadrotor simulator,” in *Conference on Robot Learning*, 2020.
- [40] Y. Song, M. Steinweg, E. Kaufmann, and D. Scaramuzza, “Autonomous drone racing with deep reinforcement learning,” in *2021 IEEE/RSJ International Conference on Intelligent Robots and Systems (IROS)*, 2021.
- [41] K. He, X. Zhang, S. Ren, and J. Sun, “Deep residual learning for image recognition,” in *Proceedings of the IEEE conference on computer vision and pattern recognition*, pp. 770–778, 2016.
- [42] P. Foehn, E. Kaufmann, A. Romero, R. Penicka, S. Sun, L. Bauersfeld, T. Laengle, G. Cioffi, Y. Song, A. Loquercio, and D. Scaramuzza, “Agilicious: Open-source and open-hardware agile quadrotor for vision-based flight,” *Science Robotics*, vol. 7, no. 67, 2022.
- [43] J. Deng, W. Dong, R. Socher, L.-J. Li, K. Li, and L. Fei-Fei, “Imagenet: A large-scale hierarchical image database,” in *2009 IEEE conference on computer vision and pattern recognition*, pp. 248–255, Ieee, 2009.
- [44] A. Szot, A. Clegg, E. Undersander, E. Wijmans, Y. Zhao, J. Turner, N. Maestre, M. Mukadam, D. Chaplot, O. Maksymets, A. Gokaslan, V. Vondrus, S. Dharur, F. Meier, W. Galuba, A. Chang, Z. Kira, V. Koltun, J. Malik, M. Savva, and D. Batra, “Habitat 2.0: Training home assistants to rearrange their habitat,” in *Advances in Neural Information Processing Systems (NeurIPS)*, 2021.

VII. APPENDIX

A. Reward Function Hyperparameters in RL

In our experiments, we employ identical hyperparameters for both state-based teacher training and vision-based RL fine-tuning to ensure a fair comparison. These parameters are determined based on iterations, shown in Table IV in both simulation and real-world experiments, aiming to achieve optimal and smooth performance for the state-based policy.

TABLE III

Reward Name	Symbol	Value
Progress reward	λ_1	0.5
Perception-aware reward	λ_2	0.025
Command smoothness reward	λ_3	$2e-4$
Body rate penalty	λ_4	$5e-4$
Gate passing reward	c_1	10
Collision penalty	c_2	4

TABLE IV: Parameters for RL training.

B. Hyperparameters in RL Adaptive Finetuning

During our adaptive fine-tuning step, we initialize LR_π with 0, LR_V with $3e-4$, and set the terminal learning rates to $LR_{\pi_{\max}}$ with $1.5e-4$, and $LR_{V_{\min}}$ with $1e-4$. An illustration of the learning rate w.r.t. the training steps is shown in Fig. 10.

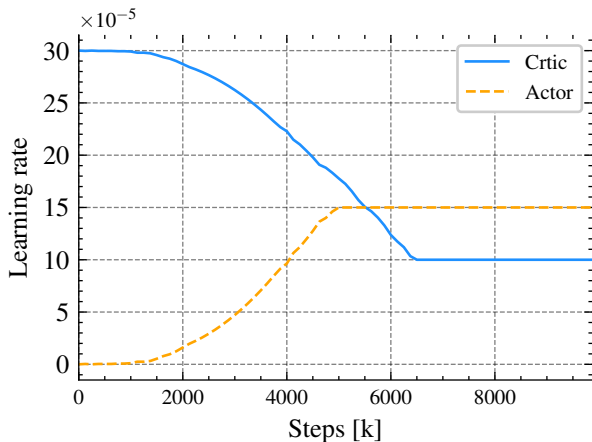


Fig. 10: Learning rate visualization of our adaptive RL fine-tuning stage.

C. Imitation Learning Performance Comparison

As we demonstrate how different stages of imitation learning policies affect fine-tuning performance, we visualize the trajectories of these policies using various percentages of the 10M budgets. In Fig. 11 (a), we observe that even with 100% data samples, behavior cloning still struggles to achieve robust flight. In contrast, DAgger exhibits promising performance, especially when using 15% of the data in Fig. 11 (b), and the training converges smoothly at 60% in Fig. 11 (c).

D. Onboard Image Visualization

To significantly reduce the sim-to-real gap, we gather LiDAR and image data within our indoor testing arena and construct a digital twin for all our experiments. In Fig 12,

visualizations of the images and the corners of our policies on three different racing tracks are depicted. It is noteworthy that for corner generation, there is a 20% probability of missing data per corner, with ± 10 pixels of noise applied. For a more detailed video showcasing real-world flights, please refer to our accompanying videos.

E. Quadrotor parameters

In this section, we introduce the quadrotor parameters utilized in real-world hardware-in-the-loop (HIL) experiments. Detailed information regarding components and physical parameters can be found in Table V. The image of the drone is demonstrated in Fig. 13.

Parameters	Agilicious platform
Thrust-to-weight Ratio	5.78
Mass [kg]	0.6
Maximum Thrust [N]	34.00
Arm Length [m]	0.15
Inertia [$g\ m^2$]	[2.50, 2.51, 4.32]
Motor Time Constant [s]	0.033
Components	Agilicious platform
Frame	Chameleon 6 inch
Motor	Xrotor 2306
Propeller	Azure Power SFP 5148 5
Flight Controller	BrainFPV radix
Battery	Tattu 4 cells 1800 mAh
Electronic Speed Controller (ESC)	Hobbywing XRotor

TABLE V: Overview of the drone parameters for real-world experiments.



Fig. 13: Our hardware drone platform for HIL experiments in the real world.

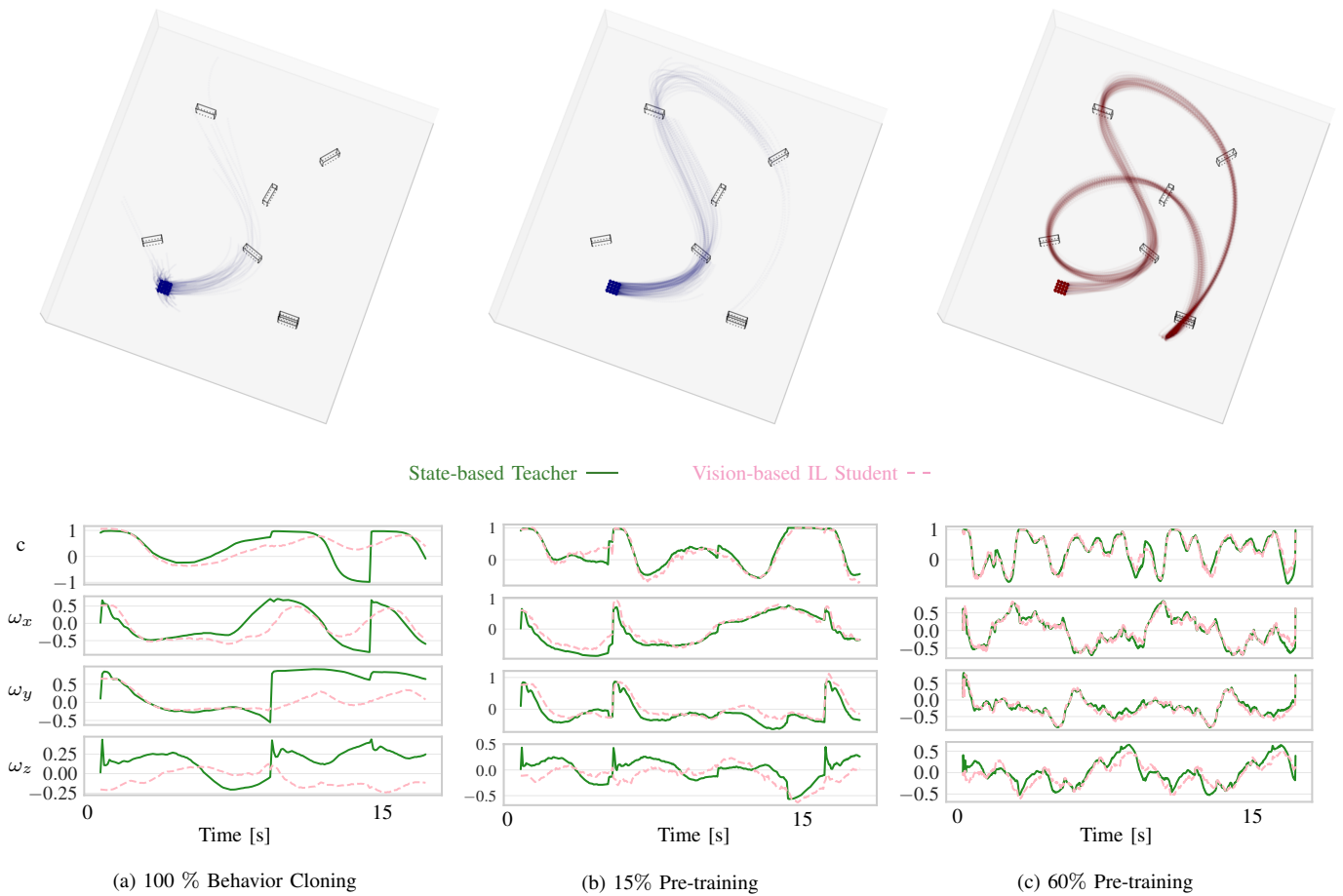


Fig. 11: *Top*: Trajectory and action errors visualization for the two different IL approaches applied to vision-based drone racing. *Bottom*: Normalized control command output visualization, from bottom to end: Collective thrust, ω_x , ω_y , ω_z , normalized in the range of $[-1, 1]$. In (a), even trained with more data samples, the policy cannot manage to consistently pass the first gate. Conversely, using DAGger, we can clearly observe that the policy could eventually fly through the gates, and using more data, the policy gets consistent improvement. All these policies are then used for the RL fine-tuning as illustrated in Fig. 7.

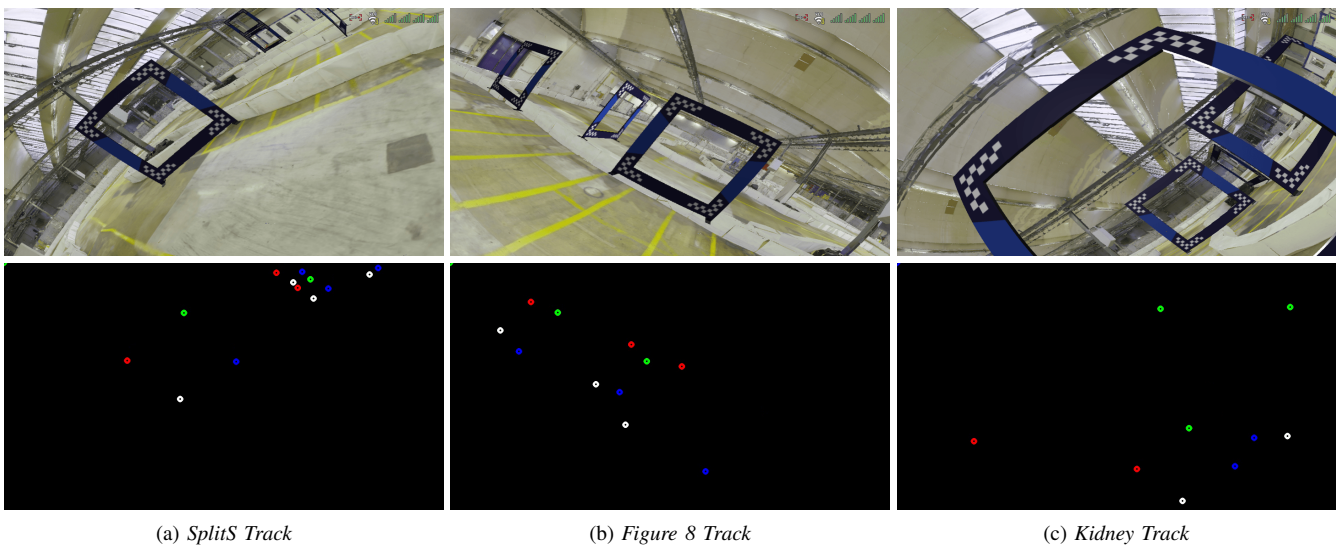


Fig. 12: *Top*: Visualization demonstrates the render image input for our visuomotor policies in simulation. *Bottom*: Sparse corners visualization. Our learned visuomotor policies, relying solely on perceptual inputs, showcase their acquired capabilities for achieving robust but agile flying performance across three distinct tracks.